

Geometric phase and a nonreciprocal spin wave circular polarizer

Yu Liu (刘瑜) and Jin Lan (兰金)*

Center for Joint Quantum Studies and Department of Physics, School of Science,
Tianjin University, 92 Weijin Road, Tianjin 300072, China and

Tianjin Key Laboratory of Low Dimensional Materials Physics and Preparing Technology, Tianjin University, Tianjin 300354, China

We show that spin wave acquires a polarization-dependent geometric phase along a cyclic trajectory of non-coplanar magnetizations in antiferromagnets. Specifically, we demonstrate that a cyclic set of 90° antiferromagnetic domain walls simultaneously introduce geometric and dynamic phases to spin wave, and thus leads to asymmetric magnitude of overall phase for left-/right-circular components. Based on the polarization-dependent phase, we propose theoretically and confirm by micromagnetic simulations that, a Mach-Zehner interferometer with cyclic 90° domain walls in one arm and homogenous domain in the other arm, naturally acts as a spin wave circular polarizer. Moreover, the circular polarizer has intrinsic nonreciprocity, which filters opposite polarization in opposite propagation direction.

Introduction. Phase is the core property of all waves, including electromagnetic wave, acoustic wave, matter wave, gravitational wave as well as spin wave. The wave phase naturally divides into two parts: the dynamical phase characterizing the wave evolution rate, and the geometric phase describing the geometric property of the wave system in parametric space [1–3]. Since its initial proposal, the concept of geometric phase has fastly evolved and become the foundation of vast and diverse disciplines [4, 5]. Exploitation of geometric phase offers new possibilities in wave manipulation including trajectory controlling, wavefront tailoring and polarization harnessing, beyond the physical limit imposed by the dynamical phase [6–13].

Spin wave, the collective precession of ordered magnetization, is an alternative angular momentum carrier beside the spin-polarized conduction electron [14–17]. The dynamical phase of spin wave can be tuned via multiple means, such as exerting magnetic field [18, 19] or electric field [20–22], passing electric current, placing magnetic impurities [23–25], coupling between two waveguides [26–28], and depositing magnetic domain walls [29–32]. Based on the dynamical phase shift, a plethora of logic and neuromorphic magnonic devices have been theoretically proposed or experimentally realized [19, 33–35].

In contrast to extensively investigated dynamical phase, the geometric phase of spin wave is only studied in limited situations. The geometric phase is shown to develop in a magnetic ring [36], between two magnetic domain walls [37] or along a magnetic helix [38] where non-coplanar magnetization forms along the spin wave trajectory. However, systematic formulation of the geometric phase for spin wave is still lacking, impeding the full exploitation of geometric phase in design of magnonic devices, let alone the collaborative leverage of geometric and dynamical phases.

In this work, we show that spin wave acquires a geometric phase cross a cyclic set of non-coplanar 90° domain walls, beside the conventional dynamical phase. By virtue of the polarization-dependent geometric phase, we propose a spin wave circular polarizer, based on the wave interference in a two-arm Mach-Zehner structure. We further show that functionality of the circular polarizer is highly reprogrammable by

reversing the propagation direction, tuning the working frequency, or altering the magnetic states. Parallel wave processings boosted by the fundamental superposition principle, are also demonstrated upon such a circular polarizer.

Polarized spin wave in antiferromagnets. Consider an antiferromagnet with the normalized Néel order denoted by unit vector \mathbf{N} , which is naturally partitioned to the static background magnetization \mathbf{n} and the dynamical spin wave \mathbf{n}' , $\mathbf{N} = \mathbf{n} + \mathbf{n}'$. Under the unity constraints $|\mathbf{N}| = 1$ and $|\mathbf{n}| = 1$, as well as the small amplitude approximation for spin wave $|\mathbf{n}'| \ll 1$, the transverse condition $\mathbf{n} \cdot \mathbf{n}' = 0$ is satisfied everywhere. Hence, it is instructive to formulate spin wave in spherical coordinates as $\mathbf{n}' = n_\theta \hat{\mathbf{e}}_\theta + n_\phi \hat{\mathbf{e}}_\phi$, where $\hat{\mathbf{e}}_{\theta/\phi}$ are two orthogonal polarization directions transverse to the back-

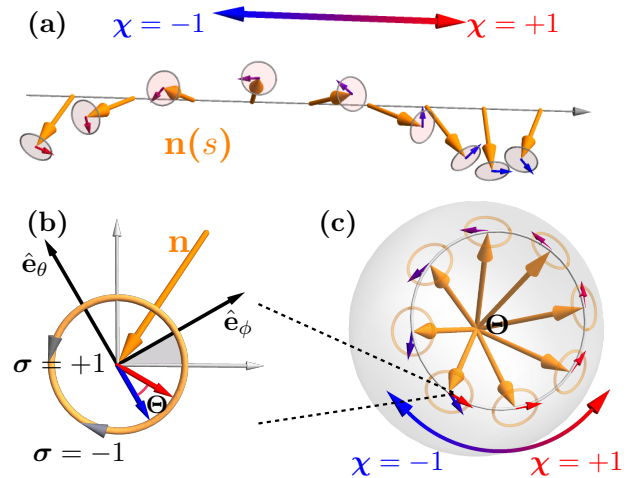


Figure 1. **Schematics of the geometric phase acquired by polarized spin wave in non-coplanar magnetizations.** (a) The evolution of the polarization direction along a closed trajectory of non-coplanar magnetizations. (b) The geometric phase of circular polarization and the rotation of linear polarization. (c) The evolution of the polarization direction in a magnetic Bloch sphere. The orange arrows are for background Néel order \mathbf{n} , and the accompanying red/blue arrows are for a specific polarization direction along trajectory.

ground magnetization $\hat{\mathbf{e}}_r \equiv \mathbf{n}$, and $n_{\theta/\phi}$ are the corresponding wave components. Alternatively, in complex form, the spin wave reads $\mathbf{n}' = \sum_{\sigma=\pm 1} \psi_{\sigma} \boldsymbol{\xi}_{\sigma}$, where $\boldsymbol{\xi}_{\sigma} = (\hat{\mathbf{e}}_{\theta} + i\sigma\hat{\mathbf{e}}_{\phi})/2$ and $\psi_{\sigma} = n_{\theta} - i\sigma n_{\phi}$ with $\sigma = \pm 1$ are bases and components of the left/right-circular polarizations, respectively.

Geometric phase of polarized spin wave. The $SO(2)$ symmetry of the linear bases $\hat{\mathbf{e}}_{\theta/\phi}$ about the background magnetization, gives rises to the $U(1)$ symmetry of the circular bases $\boldsymbol{\xi}_{\pm}$, or an indeterminate phase for the circular polarization. Hence, when a polarized spin wave travels along a closed trajectory of inhomogeneous magnetization $\mathbf{n}(s)$ parametrized by the arc length s , the circular basis may develop an additional geometric phase instead of restoring to its original phase. Specifically, the relative phase of spin wave developed between \mathbf{n} and $\mathbf{n}+d\mathbf{n}$ is characterized by the Berry connection $\Lambda_{\sigma\sigma'} = -i\boldsymbol{\xi}_{\sigma}^{\dagger} \cdot \nabla_{\mathbf{n}} \boldsymbol{\xi}_{\sigma'}$, which is diagonal in circular bases with $\Lambda_{\sigma\sigma'} = \delta_{\sigma\sigma'} \Lambda_{\sigma}$ [39]. The accompanying Berry curvature is $\Omega_{\sigma} = \nabla_{\mathbf{n}} \times \Lambda_{\sigma} = \sigma \mathbf{n}$, resembling the field radiated from a monopole of strength σ located at $\mathbf{n} = 0$. The evolution of the circular bases is then governed by $\partial_s \boldsymbol{\xi}_{\sigma} = -i(\Lambda_{\sigma} \cdot \partial_s \mathbf{n}) \boldsymbol{\xi}_{\sigma}$ with solution $\boldsymbol{\xi}_{\sigma} = \exp(i\Phi_{\sigma\chi}^G) \boldsymbol{\xi}_{\sigma}^0$, where $\boldsymbol{\xi}_{\sigma}^0$ is the initial circular basis, and χ denotes the propagation direction along the trajectory in Fig. 1(a). The geometric phase accumulated in a closed trajectory of background magnetization is thus described by

$$\Delta\Phi_{\sigma\chi}^G = - \oint_l \Lambda_{\sigma} \cdot d\mathbf{n} = -\sigma\chi\Theta, \quad (1)$$

where Θ is the magnitude of solid angle enclosed by trajectory l in a magnetic Bloch sphere, and χ corresponds to anticlockwise/clockwise circulating direction, as depicted in Fig. 1(c). The geometric phase in Eq. (1) shares a similar form to the spin-redirection phase in its optical counterpart [6, 39, 40], but the solid angle is subtended by background magnetizations here instead of optical wavevectors.

In Eq. (1), the geometric phase $\Delta\Phi_{\sigma\chi}^G$ flips sign when either the trajectory reverses its direction ($\chi \rightarrow -\chi$) or the spin wave alters its circular polarization ($\sigma \rightarrow -\sigma$), indicating its intrinsic chirality. Moreover, opposite geometric phase $\pm\Theta$ experienced by two circular modes leads to Faraday rotation of the linear bases,

$$\begin{pmatrix} \hat{\mathbf{e}}_{\theta} \\ \hat{\mathbf{e}}_{\phi} \end{pmatrix} = \begin{pmatrix} \cos \Theta & \chi \sin \Theta \\ -\chi \sin \Theta & \cos \Theta \end{pmatrix} \begin{pmatrix} \hat{\mathbf{e}}_{\theta}^0 \\ \hat{\mathbf{e}}_{\phi}^0 \end{pmatrix}, \quad (2)$$

where $\hat{\mathbf{e}}_{\theta/\phi}^0$ are the initial direction.

Geometric phase across 90° domain walls. To elaborate the concept of geometric phase, we turn to an antiferromagnet wire with magnetic cubic anisotropy [32]. The dynamics of the Néel order \mathbf{N} is governed by antiferromagnet-type Landau-Lifshitz-Gibert (LLG) equation [38, 41, 42],

$$\rho \mathbf{N} \times \ddot{\mathbf{N}} = -\mathbf{N} \times \gamma \mathbf{H} + \alpha \mathbf{N} \times \dot{\mathbf{N}}, \quad (3)$$

where ρ is the inertia of antiferromagnetic dynamics, γ is the gyromagnetic ratio, and α is Gilbert damping constant. Here

$\mathbf{H} = -\delta U/\delta \mathbf{N}$ is the effective field acting on Néel order \mathbf{N} , $U = (1/2) \int [A(\nabla \mathbf{N})^2 + K(N_x^2 N_y^2 + N_y^2 N_z^2 + N_x^2 N_z^2)] dx$ is the magnetic energy, A is the exchange stiffness, K is the cubic anisotropy strength. The inertia is expressed by $\rho = a^2/8\gamma A$, where a is the lattice constant. The dipolar field and a moderate easy-axis anisotropy do not change the main physics in this work, and thus are disregarded [43].

Due to the cubic anisotropy, the magnetization direction of a homogenous domain lies at one of the three Cartesian directions $\mathbf{n} = \hat{\mathbf{x}}_i$ with $i = \{1, 2, 3\}$. When two orthogonally magnetized $\hat{\mathbf{x}}_i$ -domain and $\hat{\mathbf{x}}_j$ -domain meet, a 90° domain wall forms with all magnetizations residing in the x_i - x_j plane. The non-coplanar magnetizations in three cyclically connected $\hat{\mathbf{x}}_i$ - $\hat{\mathbf{x}}_j$ - $\hat{\mathbf{x}}_k$ - $\hat{\mathbf{x}}_i$ domain walls subtends a solid angle of exactly $\Theta = \pi/2$ in magnitude, as depicted in Fig. 2(b). Therefore, the linear- x/y modes interchanges after traversing such a cyclic domain wall according to Eq. (2), or following the parallel transport law in a magnetic Bloch sphere as depicted in Fig. 2(b).

The spin wave evolution are further investigated by micromagnetic simulations in Mumax3 [44] with following magnetic parameters: the exchange coupling constant $A = 2.1 \times 10^{-11}$ J/m, the gyromagnetic ratio $\gamma = 2.21 \times 10^5$ m/(A s), the cubic anisotropy $K = 1.0 \times 10^4$ J/m², the damping constant $\alpha = 1.0 \times 10^{-5}$, and the lattice constant $a = 0.5$ nm. An $\hat{\mathbf{x}}$ -domain and a $\hat{\mathbf{y}}$ -domain are placed in between $\hat{\mathbf{z}}$ -domains at two sides of an antiferromagnetic wire in Fig. 2(a), and linearly polarized spin waves are injected from the left side. As shown in Fig. 2(c), after traversing two intermediate $\hat{\mathbf{x}}$ - and $\hat{\mathbf{y}}$ -domains, linear- x/y spin waves are braided by exploiting linear- z as the third state, similar to its optical and acoustic counterparts [45–47]. Nevertheless, non-Abelian braiding is absent since only two independent polarization modes exist upon any background magnetization. We have checked that the polarization braiding, as a special case of polarization rotation, is independent of spin wave frequency. In contrast, the linear- x/y spin wave remains unchanged for a trivial trajectory through the $\hat{\mathbf{z}}$ - $\hat{\mathbf{x}}$ ($\hat{\mathbf{y}}$)- $\hat{\mathbf{z}}$ domains, since the enclosing solid angle is zero therein [43].

Dynamical phase across a 90° domain wall. Beside introducing geometric phase, the domain wall also modifies the dynamical phase by altering the spin wave dynamics [29, 31, 37]. Without loss of generality, we consider a 90° domain wall lying between a $\hat{\mathbf{x}}$ -domain and a $\hat{\mathbf{y}}$ -domain, which adopts a Walker-type profile $\mathbf{n}(x) = (\sqrt{[1 - \tanh(x/W)]/2}, \sqrt{[1 + \tanh(x/W)]/2}, 0)$ with $W = \sqrt{A/K}$ the characteristic width [32, 48]. The spin wave dynamics upon such an $\hat{\mathbf{x}}$ - $\hat{\mathbf{y}}$ type 90° domain wall is then recast from the LLG equation (3) to a Klein-Gordon-like equation

$$-\frac{\rho}{\gamma} \ddot{\psi} = [-A\partial_x^2 + K + V(x)]\psi, \quad (4)$$

where $V(x) = -(11/8)K \operatorname{sech}^2(x/W)$ is the effective potential well caused by the inhomogeneous magnetization within

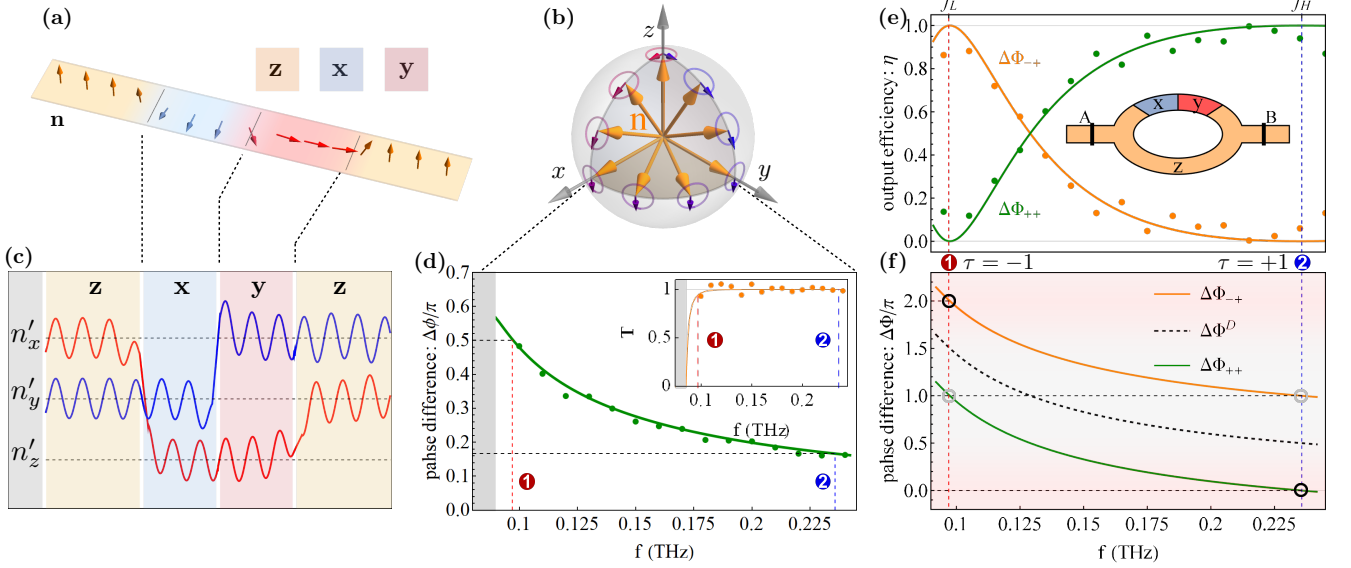


Figure 2. **Spin wave scattering and interference across the cyclic 90° domain walls.** (a) Magnetic profile of the cyclic $\hat{z}-\hat{x}-\hat{y}-\hat{z}$ domain walls. (b) Parallel transportation of a polarization direction in a magnetic Bloch sphere. (c) Braiding of linear- x/y polarizations across three 90° domain walls extracted from micromagnetic simulations. (d) Dynamical phase across a single 90° domain wall. The inset plots the transmission probability of spin wave. (e) The output efficiency of two circular polarizations. The inset depicts the schematics of the two-arm interferometer and the corresponding magnetic profiles. (f) The overall phase for left-/right circular polarizations. In (d)(e)(f), the solid lines are theoretical calculations based on Eq. (4), and the dots are extracted from micromagnetic simulations, and two circled marks are for low/high frequency.

domain wall. The deviation of $V(x)$ from the celebrated Pöschl-Teller type potential [30, 49] originates from the additional contribution of the cubic anisotropy. The hybridization of two circular modes caused by the cubic anisotropy, or the retarding effect between two linear modes [32, 43], is disregarded in Eq. (4) for model simplicity and compactness.

The spin wave scatterings by a 90° domain wall are quantitatively investigated via two numerical evaluations in parallel: the Green function calculations based on Eq. (4) via Kwant [50] and micromagnetic simulations via Mumax3 [44]. The agreements between two methods in Fig. 2(d) corroborate the following two influences caused by the potential well $V(x) < 0$ or the inhomogeneous domain wall profile $\mathbf{n}(x)$: i) A small reflection in the extremely low frequency range; ii) A positive dynamical phase $\Delta\phi > 0$ in the full range, which monotonically decreases for increasing frequency.

Overall phase across cyclic 90° domain walls. Consider a Mach-Zehner type spin wave interferometer as depicted in Fig. 2(e) inset, where a \hat{z} -domain occupies the major region, and a \hat{x} -domain and a \hat{y} -domain are deposited in the upper arm. When spin waves split from the input port converge again at the output port, the overall phase difference developed between the cyclic $\hat{z}-\hat{x}-\hat{y}-\hat{z}$ domain walls in the upper arm and the homogenous \hat{z} -domain in the lower arm is described by

$$\Delta\Phi_{\sigma\chi} = \Delta\Phi_{\sigma\chi}^G + \Delta\Phi^D = -\frac{\sigma\chi\pi}{2} + 3\Delta\phi, \quad (5)$$

where the geometric part $\Delta\Phi_{\sigma\chi}^G$ arises from the enclosing solid angle $\Theta = \pi/2$, and the dynamical part $\Delta\Phi^D$ is accumulated across three consecutive domain walls.

The frequency-dependent overall phase $\Delta\Phi^D$ in Fig. 2(f) guide us to designate binary parameter τ to following two specific frequencies: $\tau = -1$ for low frequency $f_L \approx 0.097$ THz with $\Delta\Phi^D = 3\pi/2$; and $\tau = +1$ for high frequency $f_H \approx 0.236$ THz with $\Delta\Phi^D = \pi/2$. The manipulation space $\{\sigma, \chi, \tau\}$ formed by polarization states in σ , propagation direction in χ and frequency in τ then provides 3 binary means to harness spin wave. In such a 3-bit manipulation space, the overall phase is recast from Eq. (5) to

$$\Delta\Phi_{\sigma\chi\tau} = \Delta\Phi_{\sigma\chi}^G + \Delta\Phi_{\tau}^D = \frac{2 - \tau - \sigma\chi}{2}\pi, \quad (6)$$

which is always integer multiples of π . Consequently, the interference of spin waves in two arms at the confluence region leads to the output efficiency

$$\eta_{\sigma\chi\tau} = \cos^2 \frac{\Delta\Phi_{\sigma\chi\tau}}{2} = \frac{1 + \sigma\chi\tau}{2}, \quad (7)$$

which lies in a binary on/off states, i.e., being either completely constructive $\eta = 1$ for $\Delta\Phi = 0, 2\pi$, or completely destructive $\eta = 0$ for $\Delta\Phi = \pi$, as depicted in Fig. 2(e). It is noteworthy that the on/off states possess a rather wide frequency tolerance, especially for the high-frequency case.

A non-reciprocal circular polarizer. In Eq. (7), the on/off

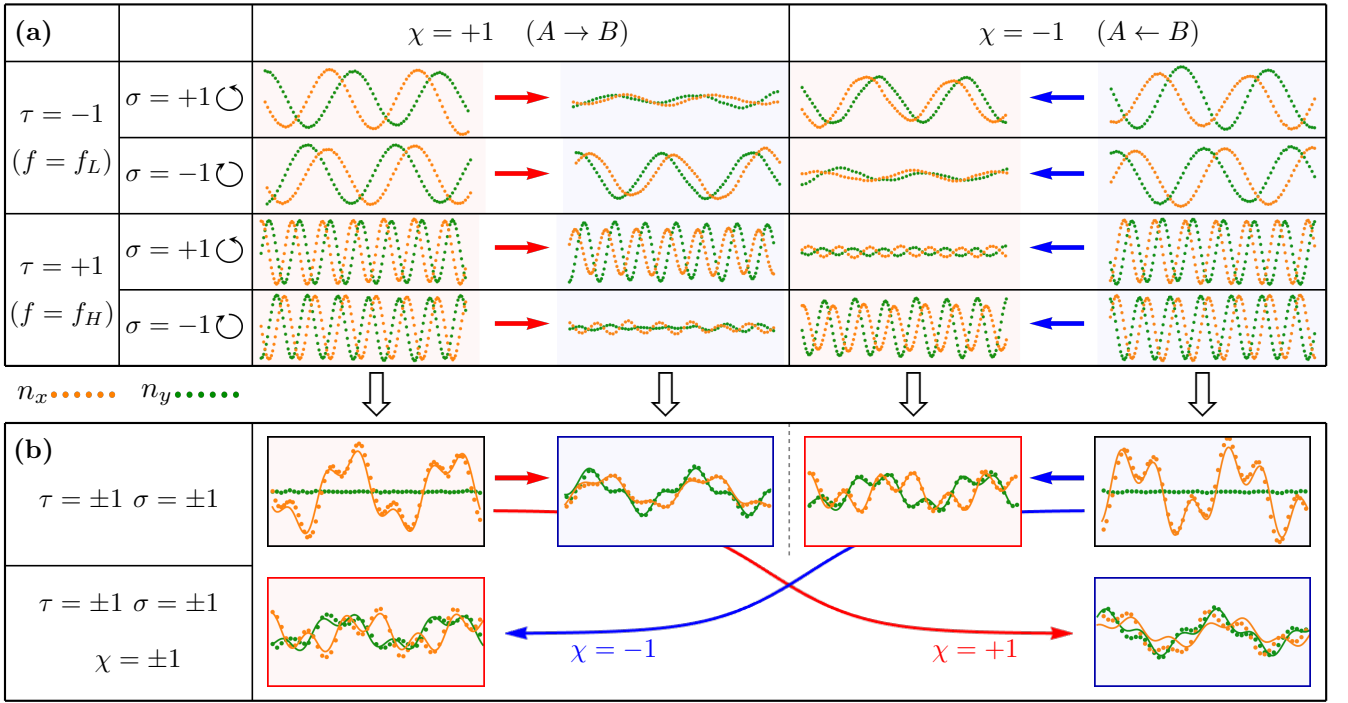


Figure 3. **Spin wave processing in a non-reciprocal circular polarizer.** (a) Individual processing in a single channel. (b) Parallel processing in multiple channels. Upper panel: unidirectional processing in 2^2 channels of $\{\sigma, \tau\}$ separately for $\chi = 1$ and $\chi = -1$; Lower panel: bidirectional processing of 2^3 channels of $\{\sigma, \tau, \chi\}$ simultaneously for $\chi = \pm 1$. In all plots, the orange/green dots are for $n_{x/y}$ extracted from micromagnetic simulations, and the solid lines are for theoretical fittings.

combinations arises in the interferometer for arbitrary binary pair in σ , χ or τ . One circular polarization is blocked $\eta_\sigma = 0$ while the other is passed $\eta_{-\sigma} = 1$, hence the two-arm interferometer acts as a spin wave circular polarizer. And when the propagation direction is reversed ($\chi \rightarrow -\chi$), the on/off state is flipped, indicating the non-reciprocity of the circular polarizer. The chirality of such a circular polarizer originates from the chiral nature of the geometric phase as manifested in Eq. (1). By switching between high/low frequency ($\tau \rightarrow -\tau$), the on/off state is flipped again, revealing a frequency-controlled chirality of the circular polarizer.

The polarization-filtering functionality of the circular polarizer is further confirmed by micromagnetic simulations in Fig. 3(a). Circular spin waves at selected frequencies are excited at A or B port of the interferometer in Fig. 2(e), and is detected in the other port. At low working frequency $f = f_L$, when two circular spin waves are continuously excited at port A , only the left-circular mode is observed at port B , signifying a left-circular polarizer in the rightward direction. In contrast, only the left-circular mode excited at port B is visible at port A , suggesting a right-circular polarizer in the leftward propagation direction. After switching to the high working frequency $f = f_H$, the right/left-circular mode is selectively passed for $A \rightarrow B$ ($A \leftarrow B$), in full compliance to the on/off rule outlined in Eq. (7).

Superposition-endorsed parallel wave processing. The principle of wave superposition not only engenders the in-

terference for waves of the same type, but also ensures that waves of different types can be brought to the same medium without mutual disturbances in linear regime [51]. Guided by this fundamental superposition principle, individual manipulations in mono-polarized, unidirectional and monochromatic fashion in Fig. 3(a) can be processed concurrently in the interferometer at once. In Fig. 3(b), when a linear-polarized and dichromatic spin wave consisting of equal components of high/low frequencies and left-/right-circular polarizations is continuously injected from port A , only the low-frequency left-circular and the high-frequency right-circular components is detected at port B . Similarly, when port B is set as the input port, the other two components are detected in port A . In both cases ($\chi = \pm 1$), the input and output signals in Fig. 3(b) are simple addition of 2^2 channels in 2-bit $\{\sigma, \tau\}$ space in Fig. 3(a).

To fully unleash the power of parallel processing, the linear-polarized and dichromatic spin wave are simultaneously excited at port A and B for finite duration of 0.16 ns. These two wave pulses travelling in opposite directions then encounter and penetrate each other, and are simultaneously detected at the other side after a waiting time 0.20 ns. Aided by the wave pulse, a parallel processing of 2^3 channels for 3-bit $\{\sigma, \chi, \tau\}$ space is enabled without much signal deterioration in this bidirectional setup, as also demonstrated in Fig. 3(b).

Magnetic programmability and scalability. By altering the magnetic states in the interferometer, the geomet-

ric/dynamical phase can be modified, and the functionality of the circular polarizer adjusts accordingly [43]. When any magnetic domain is switched $\hat{x}_i \rightarrow -\hat{x}_i$, the geometric phase $\Delta\Phi^G$ alters its sign, and thus the circular polarizer changes its chirality. Meanwhile, when magnetic domain walls along the ring formed by two arms is moved, the dynamical phase becomes $\Delta\Phi^D = d\Delta\phi$ with $d = \{-3, -1, 1, 3\}$ the number difference of domain wall in two arms, the circular polarizer at low frequency $f = f_L$ changes its filtering chirality.

The circular polarizer in this work is fully captured by two scales: the typical length $W = \sqrt{A/K}$ and the typical time $t_0 = (\pi\gamma/\sqrt{2a})\sqrt{AK}$. Hence, the whole design can be directly scaled for any combination of the exchange stiffness A and cubic anisotropy K .

Conclusion. In conclusion, we show that spin wave acquires a geometric phase along a cyclic trajectory of non-coplanar magnetizations in antiferromagnets. Moreover, a cyclic set of 90° domain walls imposes a polarization-dependent phase to passing spin wave, which consists of both geometric and dynamic phase. By virtue of such asymmetric phase for left/right-circular modes, we realize an interference-based circular polarizer. The collaboration between geometric and dynamical phase, provides new paradigms in harnessing spin wave via non-coplanar magnetizations.

Acknowledgements. J.L. is grateful to Jiang Xiao for insightful discussions. This work is supported by National Natural Science Foundation of China (Grant No. 11904260) and Natural Science Foundation of Tianjin (Grant No. 20JCQNJC02020).

* Corresponding author: lanjin@tju.edu.cn

- [1] M. V. Berry, Quantal Phase Factors Accompanying Adiabatic Changes, *Proc. R. Soc. Lond. A* **392**, 45 (1984).
- [2] R. Bhandari, Polarization of light and topological phases, *Phys. Rep.* **281**, 1 (1997).
- [3] D. Xiao, M.-C. Chang, and Q. Niu, Berry phase effects on electronic properties, *Rev. Mod. Phys.* **82**, 1959 (2010).
- [4] M. Berry, Geometric phase memories, *Nat. Phys.* **6**, 148 (2010).
- [5] E. Cohen, H. Larocque, F. Bouchard, F. Nejdassattari, Y. Gefen, and E. Karimi, Geometric phase from Aharonov–Bohm to Pancharatnam–Berry and beyond, *Nat. Rev. Phys.* **1**, 437 (2019).
- [6] K. Y. Bliokh, F. J. Rodríguez-Fortuño, F. Nori, and A. V. Zayats, Spin–orbit interactions of light, *Nature Photonics* **9**, 796 (2015).
- [7] C. P. Jisha, S. Nolte, and A. Alberucci, Geometric Phase in Optics: From Wavefront Manipulation to Waveguiding, *Laser Photonics Rev.* **15**, 2100003 (2021).
- [8] F. S. Roux, Geometric phase lens, *J. Opt. Soc. Am. A* **23**, 476 (2006).
- [9] J. Kim, Y. Li, M. N. Miskiewicz, C. Oh, M. W. Kudenov, and M. J. Escuti, Fabrication of ideal geometric-phase holograms with arbitrary wavefronts, *Optica* **2**, 958 (2015).
- [10] A. Arbabi, Y. Horie, M. Bagheri, and A. Faraon, Dielectric metasurfaces for complete control of phase and polarization with subwavelength spatial resolution and high transmission, *Nat. Nanotechnol.* **10**, 937 (2015).
- [11] M. Xiao, G. Ma, Z. Yang, P. Sheng, Z. Q. Zhang, and C. T. Chan, Geometric phase and band inversion in periodic acoustic systems, *Nat. Phys.* **11**, 240 (2015).
- [12] S. Slussarenko, A. Alberucci, C. P. Jisha, B. Piccirillo, E. Santamato, G. Assanto, and L. Marrucci, Guiding light via geometric phases, *Nat. Photonics* **10**, 571 (2016).
- [13] W. Zhu, H. Zheng, Y. Zhong, J. Yu, and Z. Chen, Wave-Vector-Varying Pancharatnam–Berry Phase Photonic Spin Hall Effect, *Phys. Rev. Lett.* **126**, 083901 (2021).
- [14] Y. Kajiwara, K. Harii, S. Takahashi, J. Ohe, K. Uchida, M. Mizuguchi, H. Umezawa, H. Kawai, K. Ando, K. Takanashi, S. Maekawa, and E. Saitoh, Transmission of electrical signals by spin-wave interconversion in a magnetic insulator, *Nature* **464**, 262 (2010).
- [15] A. V. Chumak, V. I. Vasyuchka, A. A. Serga, and B. Hillebrands, Magnon spintronics, *Nat. Phys.* **11**, 453 (2015).
- [16] L. J. Cornelissen, J. Liu, R. A. Duine, J. B. Youssef, and B. J. van Wees, Long-distance transport of magnon spin information in a magnetic insulator at room temperature, *Nat. Phys.* **11**, 1022 (2015).
- [17] A. Barman, G. Gubbiotti, S. Ladak, A. O. Adeyeye, M. Krawczyk, J. Gräfe et al., The 2021 Magnonics Roadmap, *J. Phys.: Condens. Matter* **33**, 413001 (2021).
- [18] M. P. Kostylev, A. A. Serga, T. Schneider, B. Leven, and B. Hillebrands, Spin-wave logical gates, *Appl. Phys. Lett.* **87**, 153501 (2005).
- [19] T. Schneider, A. A. Serga, B. Leven, B. Hillebrands, R. L. Stamps, and M. P. Kostylev, Realization of spin-wave logic gates, *Appl. Phys. Lett.* **92**, 022505 (2008).
- [20] T. Liu and G. Vignale, Electric Control of Spin Currents and Spin-Wave Logic, *Phys. Rev. Lett.* **106**, 247203 (2011).
- [21] X. Zhang, T. Liu, M. E. Flatté, and H. X. Tang, Electric-Field Coupling to Spin Waves in a Centrosymmetric Ferrite, *Phys. Rev. Lett.* **113**, 037202 (2014).
- [22] R. Cheng, M. W. Daniels, J.-G. Zhu, and D. Xiao, Antiferromagnetic Spin Wave Field-Effect Transistor, *Sci. Rep.* **6**, 24223 (2016).
- [23] O. V. Dobrovolskiy, R. Sachser, S. A. Bunyaev, D. Navas, V. M. Bevez, M. Zelent, W. Śmigaj, J. Rychlý, M. Krawczyk, R. V. Vovk, M. Huth, and G. N. Kakazei, Spin-Wave Phase Inverter upon a Single Nanodefekt, *ACS Appl. Mater. Interfaces* **11**, 17654 (2019).
- [24] W. Yu, J. Lan, and J. Xiao, Magnetic Logic Gate Based on Polarized Spin Waves, *Phys. Rev. Appl.* **13**, 024055 (2020).
- [25] Q. Wang, A. V. Chumak, and P. Pirro, Inverse-design magnonic devices, *Nat. Commun.* **12**, 2636 (2021).
- [26] Q. Wang, P. Pirro, R. Verba, A. Slavin, B. Hillebrands, and A. V. Chumak, Reconfigurable nanoscale spin-wave directional coupler, *Sci. Adv.* **4**, e1701517 (2018).
- [27] Q. Wang, M. Kewenig, M. Schneider, R. Verba, F. Kohl, B. Heinz, M. Geilen, M. Mohseni, B. Lägél, F. Ciubotaru, C. Adelman, C. Dubs, S. D. Cotofana, O. V. Dobrovolskiy, T. Brächer, P. Pirro, and A. V. Chumak, A magnonic directional coupler for integrated magnonic half-adders, *Nat. Electron.* **3**, 765 (2020).
- [28] M. Zhao, X.-g. Wang, Z. Luo, Q.-l. Xia, Y.-z. Nie, R. Xiong, and G.-h. Guo, Reconfigurable Spin-Wave Coupler Based on Domain-Wall Channels, *Phys. Rev. Appl.* **17**, 064013 (2022).
- [29] R. Hertel, W. Wulfhekel, and J. Kirschner, Domain-Wall Induced Phase Shifts in Spin Waves, *Phys. Rev. Lett.* **93**, 257202 (2004).
- [30] J. Lan, W. Yu, and J. Xiao, Antiferromagnetic domain wall as spin wave polarizer and retarder, *Nat. Commun.* **8**, 178 (2017).
- [31] J. Han, P. Zhang, J. T. Hou, S. A. Siddiqui, and L. Liu, Mutual control of coherent spin waves and magnetic domain walls in a

- magnonic device, *Science* **366**, 1121 (2019).
- [32] F. Ye and J. Lan, Magnetically switchable spin-wave retarder with 90 degree antiferromagnetic domain wall, *Phys. Rev. B* **104**, L180401 (2021).
- [33] Á. Papp, W. Porod, and G. Csaba, Nanoscale neural network using non-linear spin-wave interference, *Nat. Commun.* **12**, 6422 (2021).
- [34] P. Pirro, V. I. Vasyuchka, A. A. Serga, and B. Hillebrands, Advances in coherent magnonics, *Nat. Rev. Mater.* , 1 (2021).
- [35] A. V. Chumak, P. Kabos, M. Wu, C. Abert, C. Adelman, A. O. Adeyeye et al., Advances in Magnetism Roadmap on Spin-Wave Computing, *IEEE Trans. Mag.* **58**, 1 (2022).
- [36] V. K. Dugaev, P. Bruno, B. Canals, and C. Lacroix, Berry phase of magnons in textured ferromagnets, *Phys. Rev. B* **72**, 024456 (2005).
- [37] F. J. Buijnsters, Y. Ferreiros, A. Fasolino, and M. I. Katsnelson, Chirality-Dependent Transmission of Spin Waves through Domain Walls, *Phys. Rev. Lett.* **116**, 147204 (2016).
- [38] H. Wu and J. Lan, Curvilinear manipulation of polarized spin waves, *Phys. Rev. B* **105**, 174427 (2022).
- [39] M. Onoda, S. Murakami, and N. Nagaosa, Hall Effect of Light, *Phys. Rev. Lett.* **93**, 083901 (2004).
- [40] K. Y. Bliokh, M. A. Alonso, and M. R. Dennis, Geometric phases in 2D and 3D polarized fields: Geometrical, dynamical, and topological aspects, *Rep. Prog. Phys.* **82**, 122401 (2019).
- [41] F. D. M. Haldane, Nonlinear Field Theory of Large-Spin Heisenberg Antiferromagnets: Semiclassically Quantized Solitons of the One-Dimensional Easy-Axis Néel State, *Phys. Rev. Lett.* **50**, 1153 (1983).
- [42] E. G. Tveten, A. Qaiumzadeh, and A. Brataas, Antiferromagnetic Domain Wall Motion Induced by Spin Waves, *Phys. Rev. Lett.* **112**, 147204 (2014).
- [43] See Supplementary Materials for detailed derivation of antiferromagnetic LLG equation, the setup of micromagnetic simulations, the influence of dipolar field and easy-axis anisotropy, the magnetic programmability of circular polarizer, and the truth table of circular polarizer in full state space.
- [44] A. Vansteenkiste, J. Leliaert, M. Dvornik, M. Helsen, F. Garcia-Sanchez, and B. Van Waeyenberge, The design and verification of MuMax3, *AIP Adv.* **4**, 107133 (2014).
- [45] T. Iadecola, T. Schuster, and C. Chamon, Non-Abelian Braiding of Light, *Phys. Rev. Lett.* **117**, 073901 (2016).
- [46] X.-L. Zhang, F. Yu, Z.-G. Chen, Z.-N. Tian, Q.-D. Chen, H.-B. Sun, and G. Ma, Non-Abelian braiding on photonic chips, *Nat. Photon.* **16**, 390 (2022).
- [47] Z.-G. Chen, R.-Y. Zhang, C. T. Chan, and G. Ma, Classical non-Abelian braiding of acoustic modes, *Nat. Phys.* **18**, 179 (2022).
- [48] E. G. Tveten, A. Qaiumzadeh, O. A. Tretiakov, and A. Brataas, Staggered Dynamics in Antiferromagnets by Collective Coordinates, *Phys. Rev. Lett.* **110**, 127208 (2013).
- [49] W. Yu, J. Lan, and J. Xiao, Polarization-selective spin wave driven domain-wall motion in antiferromagnets, *Phys. Rev. B* **98**, 144422 (2018).
- [50] C. W. Groth, M. Wimmer, A. R. Akhmerov, and X. Waintal, Kwant: A software package for quantum transport, *New J. Phys.* **16**, 063065 (2014).
- [51] D. H. Goldstein, *Polarized Light*, 3rd ed. (CRC Press, Boca Raton, 2017).